Experimental and Numerical Testing of a Multi-Modular Floating Structure with Varying Connection Stiffness

Trine Aas-Hansen * **Vegard Njøten Fagerbakke** **
Trygve Kristiansen ** **Svein Sævik** ** **Dong Trong Nguyen** ***

* *Norwegian University of Science and Technology, Trondheim, Norway (e-mail: trine.aas-hansen@ntnu.no).*
** *Norwegian University of Science and Technology, Trondheim, Norway*
*** *Norwegian University of Science and Technology, Trondheim, Norway(e-mail: dong.t.nguyen@ntnu.no).*

Abstract:
This work is a step towards conceptualizing a smart multi-modular structure, whose main application is solar energy harvest, with the innovative idea of connectors that can be controlled to mitigate motions and loads in a changing environment. The paper presents selected preliminary results from experimental tests of an array of floating column-based modules exposed to regular waves of different periods. Each pair of neighboring modules was connected by two spring connectors with both tension and compression stiffness. The paper presents an investigation of motion responses versus load frequencies corresponding to four tested spring stiffnesses.
The model test results serve as a basis for validating a numerical model that is implemented for control design and simulation purposes. Wave-, mooring- and connector forces are considered in the simulations. The proposed method will act as a tool for further evaluation of the effect of changing the connection stiffness according to the incoming waves and the investigation of whether it is beneficial to apply a smart connector that can adapt to varying sea states.

Keywords: Renewable Energy, Floating Solar, Model Testing, Numerical Modelling, Control

1. INTRODUCTION

1.1 Background

The world demands more green energy to reduce the global carbon emissions. To replace polluting energy sources, a large variety of sustainable solutions is essential. According to the Intergovernmental Panel on Climate Change, solar photovoltaic (PV) has become a competitive energy source as the cost has decreased by 85 % between 2010 and 2019 (IPCC, 2023). In areas where solar irradiation is abundant, but available land areas are in high demand, building floating solar plants could be a valuable contribution towards the energy transition. In addition to the advantage of not using land areas, Kumar et al. (2021) summarized benefits of floating solar, including better cooling effect, reduction of water evaporation and less accumulation of dust.

If floating large-area structures can be designed to sustain higher environmental loads in an exposed or offshore environment, new solutions for floating photovoltaic (FPV) power plants can be investigated. DNV (2022) listed the main opportunities for FPV as; making use of abundant solar energy in more areas; maximizing the use of space and existing infrastructure by combining FPV with for instance offshore wind installations; provide offshore charging for electric marine vessels or for production of alternative fuels; supplying green energy to islands or maritime industry; and finally, the reuse of competence from other marine industries.

Placing floating structures in harsher offshore environments with wind, current and changing wave states is not a new research topic. The oil and gas industry has designed and built offshore installations for decades. Ideas for very large floating structures (VLFSs) explores making large areas available on water surfaces for e.g. buildings, floating ports, airports and agriculture (Lamas-Pardo et al., 2015). To reduce bending moments on these large-area structures, connecting several smaller modules together to make a flexible structure that is allowed to move with the changing sea surface could be a solution. Such multi-modular structures, in a smaller scale than the VLFSs, will in this paper be investigated for the purpose of solar harvest in exposed areas.

A nonlinear model of connected floating modules using network theory has been used to analyze the response and connection loads of a multi-modular structure (Zhang

⋆ The PhD position of the first author is funded by Department of Marine Technology at NTNU. This work was partly supported by the Research Council of Norway through SFI BLUES, grant number 309281.

et al., 2015). Shi et al. (2018) validated the network modelling method by experimental testing of three modules in an array, and Ding et al. (2021) by full scale results from the Scientific Research and Demonstration Platform in the South China Sea.

Multi-modular structures introduce connection points which present weak links in terms of fatigue life and durability. This motivates research on how to reduce relative module motion and loads in connections when such structures are exposed to changing environmental conditions. The motion response and oscillations as well as connector loads of a multi-modular structure were shown by Jiang et al. (2021) to be affected by the connector stiffness between modules. By adapting this stiffness to different wave periods, studies have shown that it is possible to retain the structure in a state where oscillations are kept at a minimum, also known as amplitude death state (Xu et al., 2014; Xia et al., 2016; Zhang et al., 2017). By actively controlling their stiffness, the connectors themselves can be used as actuators.

This paper investigates a type of multi-modular structure with modules larger than the components of typical floating solar rafts, but smaller than the modules in very large floating structures. Further, this paper contributes to research by including varying connector stiffness in both numerical and experimental tests. The main objectives are to analyze the behavior of different configurations of multi-modular structures, investigate the effect of different connector stiffness and to validate a numerical simulator by comparable experimental results. The motivation for the work is to prepare for development of a control system that changes the dynamics of the structure as a response to the current sea state by using active control of the stiffness in connection points. The work utilizes existing numerical and experimental modelling techniques on a new type of structure and, by creating a modeling framework, contributes towards an evaluation of the idea of creating smart multi-modular structures that adapt to changing environmental conditions.

1.2 Paper Outline

The paper starts with Sect. 2 presenting a test case with necessary parameters for both the experimental and simulator setup. It describes how the test case is adapted for model testing and introduces the mathematical modelling of the dynamical system. Results are presented in Sect. 3 and concluding remarks are given in Sect. 4.

2. CASE STUDY

2.1 Test Case

A common test case is used in both the experimental and numerical investigation for easy comparison. This case is based on an offshore floating solar power concept, utilizing the same modules as used in previous model tests (Onsrud, 2019). Square rigid platforms with four cylindrical floaters or columns (Fig. 1) are flexibly connected to form an interconnected large-area structure. Arrays of 1, 2, 3 and 5 modules are subjected to regular waves in the longitudinal direction and are tested with varying stiffness in the connection points. Table 1 presents the full-scale parameters of the test case.

Table 1. Test case parameters (full scale)

Parameter			Unit
Module size	$L \times W$	12×12	[m]
Module mass	m	9088	[kg]
Draft	d	1.13	[m]
Column radius	r	0.8	[m]
Column height	h	2.63	[m]
CG	(x_g, y_g, z_g)	(0,0,-1.3)	[m]
CF	(x_f, y_f, z_f)	(0,0,0)	[m]
CB	(x_b, y_b, z_b)	(0,0,d/2)	[m]
Module distance	Δx	1.3	[m]
No. of modules	N	1-5	[-]
No. of mooring lines	N_m	4	[-]
No. of connectors between neighbors	N_c	2	[-]
Mooring line stiffness	K_m	2800	[N/m]
Connector stiffnesses:	K_c	6-29	[kN/m]
- Conn. stiffness S1		29000	[N/m]
- Conn. stiffness S2		26000	[N/m]
- Conn. stiffness S3		15000	[N/m]
- Conn. stiffness S4		6000	[N/m]
Wave period	T_w	2.0-8.0	[s]
Wave steepness	H/λ	1/116	[-]
Water density	ρ	1000	[kg/m^3]

Table 2. Run overview

Parameter	Variations
Module configurations:	1×1, 2×1, 3×1, 5×1
Connector stiffness:	S1, S2, S3, S4, Hinge*
Wave period:	2.0-8.0 s
	**Only model test with configuration 2×1 and 5×1*

2.2 Model Test

The model tests were performed in a towing tank at NTNU in Trondheim, Norway. The tank is 2.8 by 25 meters, with a water depth of 0.7 meters. It has a wave maker and a wave beach to absorb energy from the waves. The model was Froude scaled by 1:20 according to the parameters presented in Table 1. Figure 2 shows a photo of the model test setup for the three-module configuration in the towing tank where the experiments were performed.

The first and last module in each test configuration were moored in four corners by pre-tensioned springs (Figs. 1 and 2). All modules are thus kept in a neutral position in calm water. Each pair of modules was connected by two spring connectors (Figs. 3 and 4) functioning with both tension and compression stiffness. Tests were performed according to Table 2. Each combination of connector type and number of modules was exposed to regular waves travelling in the negative x-direction. The wave period was limited by the water depth in the tank, ensuring linear wave behavior.

The response of each module was tracked in six degrees of freedom (DOFs) using a camera-based motion capture system. Load cells were used to measure the force in local x-direction in one spring of each connection pair, see Fig. 3. The wave height was measured by wave probes at 8 different locations throughout the tank.

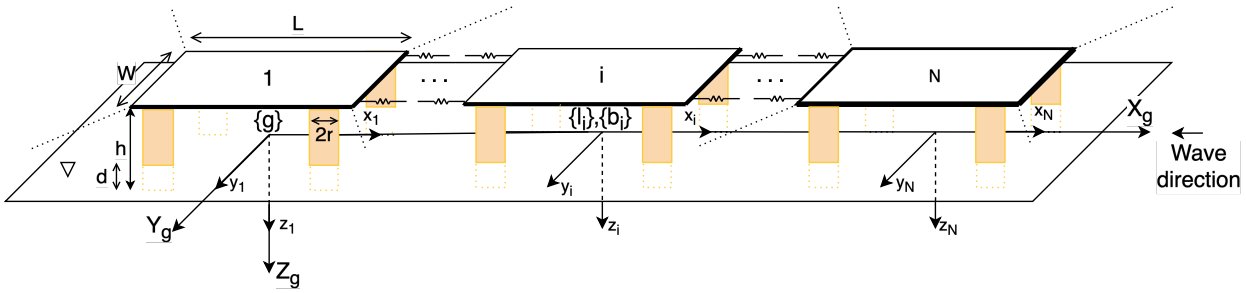

Fig. 1. General overview of the test case. Module numbering and global reference frame $\{g\} = (X_g, Y_g, Z_g)$, as well as selected parameters from Table 1 are presented. The local $\{l_i\}$ and body-fixed $\{b_i\}$ reference frames coincides when the modules are in neutral position. Further, connection springs are indicated between modules, and mooring lines are indicated as dotted lines in the corners of the end modules.

The results from this model test have also been evaluated in a master thesis from NTNU by Fagerbakke (2023).

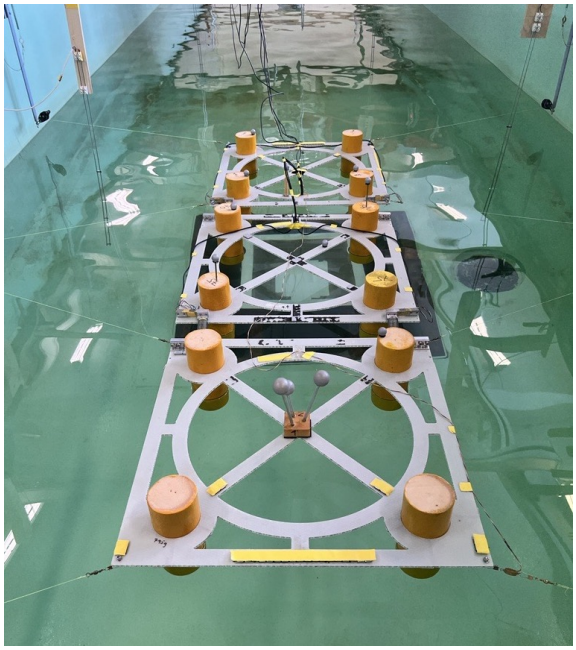

Fig. 2. Model test setup, N=3.

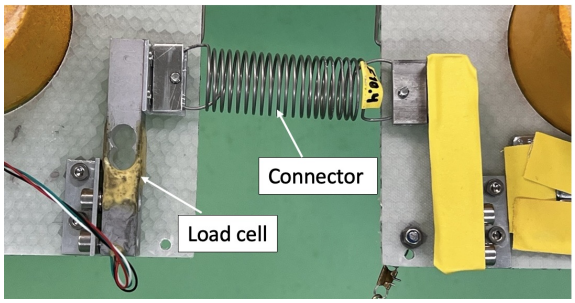

Fig. 3. Model test connector and load cell.

2.3 Modelling of the Test Case

The numerical model is based on a mathematical description of rigid modules with flexible connections.The main assumptions for the numerical model are:

Assumption 1. The modules are assumed rigid.

Assumption 2. Waves are modelled as linear deep-water waves, unaffected by shallow-water effects

Assumption 3. Motions in xy-plane are assumed small, thus reducing the analysis to a 2D-problem.

Assumption 4. Connector springs between the modules are limited to axial forces.

Assumption 5. The effect of finite column length is neglected.

Assumption 6. Modules are allowed to overlap if motions are large, collisions are not modelled.

Reference Frames: Three types of reference frames were used to model the multi-modular island, see Fig. 1. A global inertial reference frame defined by $\{g\} = (X_g, Y_g, Z_g)$, where X_g and Y_g is zero in the initial position of the geometrical center of the first module, and Z_g is zero at the water surface, with positive axis downwards. A local coordinate system $\{l_i\} = (x_i^l, y_i^l, z_i^l)$ has its origin in the neutral position of each module. In addition, each module has its own body-fixed reference frame, $\{b_i\} = (x_i^b, y_i^b, z_i^b)$, also with the positive z-axis down from the sea surface.

The position and orientation vector for a 6 DOF module i, in its local reference frame is defined as $\boldsymbol{\eta}_i = [\boldsymbol{p}_i^\top, \boldsymbol{\Theta}_i^\top]^\top$, where $\boldsymbol{p}_i = [x_i, y_i, z_i]^\top$ represent the module's x-, y- and z-position in $\{l_i\}$, and $\boldsymbol{\Theta}_i = [\phi_i, \theta_i, \psi_i]^\top$ represent the orientation of $\{b_i\}$ in $\{l_i\}$ in roll, pitch and yaw respectively. The velocity in the body-fixed reference frame of each module is $\boldsymbol{\nu}_i = [u_i, v_i, w_i, p_i, q_i, r_i]^\top$ representing translational velocities in x, y and z (u_i, v_i, w_i), and rotational velocities around these axes (p_i, q_i, r_i).

The transformation between two reference frames is described by $\dot{\boldsymbol{\eta}}_i = \boldsymbol{J}(\boldsymbol{\Theta}_i)\boldsymbol{\nu}_i$ with the transformation matrix $\boldsymbol{J}(\boldsymbol{\Theta})$ being a block diagonal matrix defined by the transformation of translations, $\boldsymbol{R}(\boldsymbol{\Theta})$, and rotations, $\boldsymbol{T}(\boldsymbol{\Theta})$, according to Fossen (2021).

Equation of Motion: The equation of motion for module i in its body-fixed frame $\{b_i\}$ is given by

$$\boldsymbol{M}_i(\omega)\dot{\boldsymbol{\nu}}_i + \boldsymbol{D}_i(\omega)\boldsymbol{\nu}_i + \boldsymbol{J}^\top(\boldsymbol{\Theta}_i)\boldsymbol{C}_i\boldsymbol{\eta}_i = \boldsymbol{F}_i^b(\omega),\ i = 1, ..., N \tag{1}$$

$\boldsymbol{M}_i(\omega)$ includes the rigid body mass matrix $\boldsymbol{M}_{RB,i}$ and hydrodynamic added mass $\boldsymbol{A}_i(\omega)$. The force vector $\boldsymbol{F}_i^b$ is the sum of connector forces $\boldsymbol{F}_{c,i}^b$, mooring forces $\boldsymbol{F}_{m,i}^b$, and wave loads $\boldsymbol{F}_{w,i}^b(\omega)$. $\boldsymbol{D}(\omega)_i$ and $\boldsymbol{C}_i$ represents potential damping and restoring matrices respectively.

Wave Loads: The wave loads are modeled as potential linear excitation loads, $\boldsymbol{F}^b_{pot.,i}(\omega)$, and hydrodynamic drag, $\boldsymbol{F}^b_{morison,i}(\omega)$. The potential wave loads can be expressed as

$$\boldsymbol{F}^b_{pot.,i} = \bar{\boldsymbol{F}}_{pot.,i}(\omega)\cos\left(\omega_w t - k x^g_{lg,i} + \alpha_i\right) \tag{2}$$

The amplitude, $\bar{\boldsymbol{F}}_{pot.,i}(\omega)$, and phase angle, $\alpha_i(\omega)$, are calculated with help from WADAM (DNV-GL, 2017). k is the wave number, defined by $k = \omega^2/g$, where g is the gravity acceleration. $x^g_{lg,i}$ is the position of the local reference frame of the module in the global reference frame. To account for viscous effects, drag loads are added through Morison's equation in vertical and horizontal directions. Drag forces and moments are calculated using strip theory and the crossflow principle for each column $i.p$:

$$\begin{aligned} \boldsymbol{f}^b_{morison,i.p} &= \int \frac{1}{2}\rho C_D 2r|\boldsymbol{u}_{r,i.p}|\boldsymbol{u}_{r,i.p}dz \\ \boldsymbol{m}^b_{morison,i.p} &= \boldsymbol{r}_{i.p} \times \boldsymbol{f}^b_{morison,i.p} \end{aligned} \tag{3}$$

where C_D is the drag coefficient, $\boldsymbol{u}_{r,i}$, is the relative velocity vector on the column and $\boldsymbol{r}_{i.p}$ is the distance between the body frame origin and the force application point. The total drag load is the sum of loads on all N_p columns on the module:

$$\boldsymbol{F}^b_{morison,i} = \sum_{p=1}^{N_p} \begin{bmatrix} \boldsymbol{f}^b_{morison,i.p} \\ \boldsymbol{m}^b_{morison,i.p} \end{bmatrix} \tag{4}$$

Connector Loads: The moving neighboring modules will impose forces on each other based on the distance between connection points and the spring stiffness of the connector. Following Assumptions 3 and 4, forces occurring from movement along the transversal and vertical direction (i.e. along y and z) are neglected, thus the connector forces are a result of movement in x-direction. The numbering of the four connectors of module i is presented in Fig. 4.

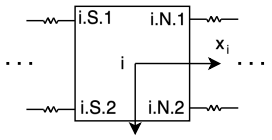

Fig. 4. Connectors 1-4 on module i. N indicates the north face of the module, S indicates the south face.

The total connection force on module i is given by

$$\boldsymbol{F}^b_{c,i} = \sum_{j=1}^{N} \sum_{\substack{m\in\mathcal{M} \\ o\in\mathcal{O}}} \Phi_{m,ij}\boldsymbol{K}_c(\boldsymbol{p}_i,\boldsymbol{p}_j)_{m,o}, \begin{cases} \mathcal{M} & = [\text{N,S}] \\ \mathcal{O} & = [\text{S,N}] \end{cases} \tag{5}$$

where $\boldsymbol{\Phi}_m \in \mathbb{R}^{N\times N}$ represent the topology matrices for the m face of the modules. $\Phi_{\text{N},ij}$ is 1 if the north face of module i is connected to module j, and 0 if not. Further, $\boldsymbol{K}_c(\boldsymbol{p}_i,\boldsymbol{p}_j)_{m,o}$ is given by

$$\boldsymbol{K}_c(\boldsymbol{p}_i,\boldsymbol{p}_j)_{m,o} = \sum_{k=1}^{N_c} \begin{bmatrix} \boldsymbol{f}^b_c(\boldsymbol{p}_i,\boldsymbol{p}_j)_{m,o,k} \\ \boldsymbol{r}_{c,i.m.k} \times \boldsymbol{f}^b_c(\boldsymbol{p}_i,\boldsymbol{p}_j)_{m,o,k} \end{bmatrix} \tag{6}$$

where

$$\boldsymbol{f}_c(\boldsymbol{p}_i,\boldsymbol{p}_j)_{m,o,k} = -K_c(\boldsymbol{p}^l_{i.m.k} - \boldsymbol{p}^l_{j.o.k} - \boldsymbol{p}_0) \tag{7}$$

Simplified to consider motion in x-direction only:

$$\boldsymbol{K}_c(\boldsymbol{p}_i,\boldsymbol{p}_j)_{m,o} = -K_c\sum_{k=1}^{N_c}[(x^g_{i.m.k} - x^g_{j.o.k} - \delta x), 0, 0, 0, 0, 0]^\top \tag{8}$$

where δx is the neutral distance between modules in x-direction.

Mooring Loads: Mooring stiffness is implemented with only one connection point moving, and the other fixed in a simulated anchoring point. The force and moment from mooring line k_m on module i are given by

$$\begin{aligned} \boldsymbol{f}^l_{m,i.k_m} &= (K_m(\|\boldsymbol{l}_{i.k_m}\| - L_{k_m}) + f_{pt,k_m})\frac{\boldsymbol{l}_{i.k_m}}{\|\boldsymbol{l}_{i.k}\|} \\ \boldsymbol{m}^b_{m,i.k_m} &= \boldsymbol{r}^b_{m,i.k_m} \times \boldsymbol{J}^\top(\boldsymbol{\Theta}_i)\boldsymbol{f}^l_{m,i.k_m} \end{aligned} \tag{9}$$

where f_{pt,k_m} is the pretension in the mooring line, $\boldsymbol{l}_{i.k_m}$ is the vector describing the relative position of mooring point and the anchoring point, L_{k_m} is the initial length of mooring line k_m and $\boldsymbol{r}^b_{m,i.k_m}$ is the lever arm to the point where mooring line k_m is connected to module i.

The total mooring load on module i is the sum of forces and moments from all N_m mooring lines connected to it:

$$\boldsymbol{F}^b_{m,i} = \sum_{k_m=1}^{N_m} \Phi_i \begin{bmatrix} \boldsymbol{f}^b_{m,i.k_m} \\ \boldsymbol{m}^b_{m,i.k_m} \end{bmatrix}, \; i = 1, ..., N \tag{10}$$

where $\boldsymbol{\Phi} \in \mathbb{R}^N$ and Φ_i is equal to 1 if module i is moored, and 0 if it is not.

3. RESULTS AND DISCUSSION

3.1 Natural Periods

Table 3. N = 2, Calculated undamped natural periods (mass + added mass 1.5e4)

	$K_c = S1$	$K_c = S2$	$K_c = S3$	$K_c = S4$
T_{n1} [s]	11.8	11.8	11.8	11.8
T_{n2} [s]	2.2	2.3	3.0	4.5

Table 4. N = 3, Calculated undamped natural periods in surge (mass + added mass 1.5e4)

	$K_c = S1$	$K_c = S2$	$K_c = S3$	$K_c = S4$
T_{n1} [s]	14.5	14.5	14.5	14.7
T_{n2} [s]	3.1	3.2	4.2	5.9
T_{n3} [s]	1.8	1.9	2.6	3.8

Table 3 presents the estimated full scale undamped natural periods in surge of a 1 DOF system with 2 modules and with different stiffness of the connector spring. T_{n1} corresponds to the mode shape where both modules are moving in the same direction, while T_{n2} corresponds to motion in opposite directions.

Natural periods for a system with 3 modules are presented in Table 4. T_{n1} corresponds to all modules moving in the same direction. T_{n2} corresponds to the middle module at a standstill, while the two end modules move in opposite directions causing large relative motion in both connection pairs. T_{n3} is the natural period of the mode shape where the first and third modules move in the same direction, but opposite the middle. Based on the nature of these mode

shapes, the relative motion, and thus the connector force, is expected to be largest at T_{n2} and T_{n3}.

Finally, the mode shapes for the five-module configuration are similar to the three-module case. With more modules, there are more mode shapes and possible resonance periods, and it becomes less evident which wave periods will lead to the largest mean connection load amplitudes.

The first natural periods are corresponding to global surge motion of the island and are not expected to lead to significant relative motion. These were calculated to be outside the interval of wave periods that have been investigated, and T_{n1} will thus not be discussed further in this work.

Heave natural period for a single module due to hydrostatic restoring force is estimated to be 2.7 s.

3.2 Stiffness Dependence in Model Test

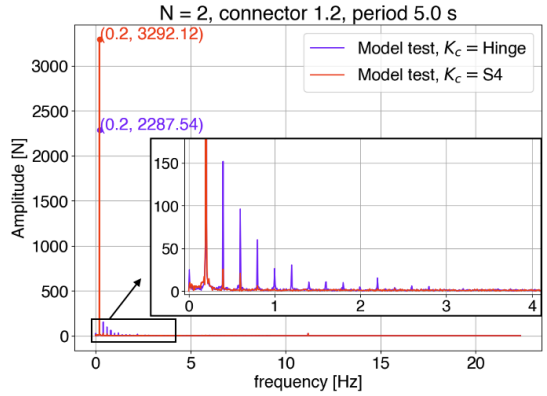

(a) N=2

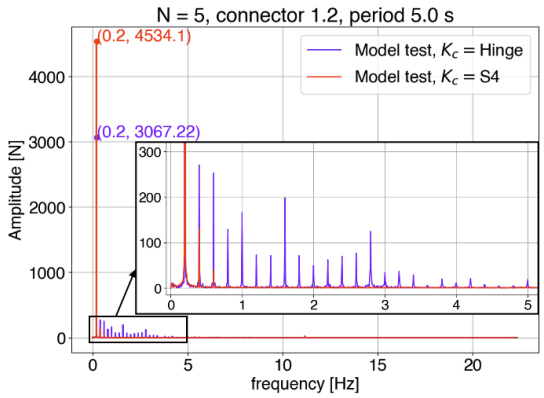

(b) N=5

Fig. 5. Measured higher harmonic forces in one connector between module 1 and 2. Hinged connection compared to the softest spring connection, stiffness $K_c = S4$.

Connector loads are plotted in frequency domain in Figs. 5(a) (N=2) and 5(b) (N=5) for wave period $T_w = 5.0$ s. To highlight the effect of the connector stiffness, these figures present two extreme cases: the hinged connector and the softest spring connector, $S4$. Although amplitudes at the wave frequency are higher, the softer spring appears to transfer little to no forces at higher frequencies.

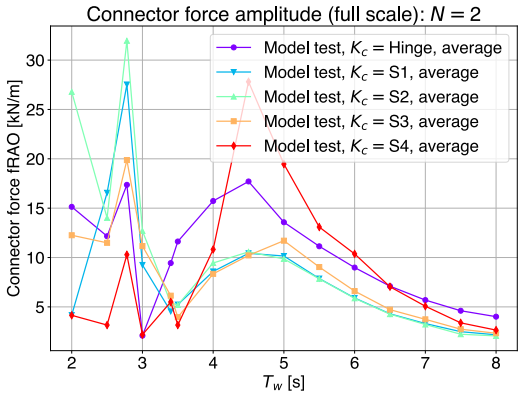

(a) N=2

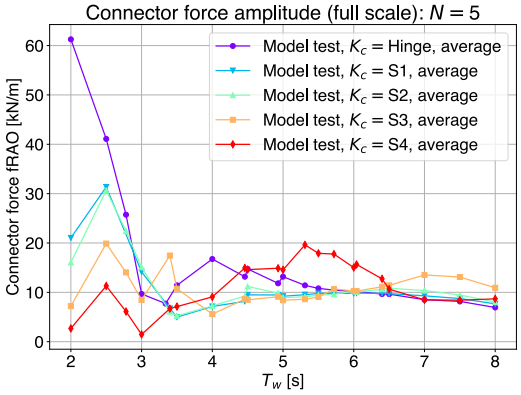

(b) N=5

Fig. 6. Average connector force all connectors.

Figures 6(a) and 6(b) present connector forces in the local x-direction for N=2 and N=5 configurations respectively. The hinged connector generally yields higher connector loads than the tests where modules are connected by springs. It appears beneficial with a softer connection at lower wave periods, while for longer periods the stiffer springs are preferable to avoid the resonance peak related to T_{n2}.

As mentioned in Sect. 2.2, the first and last module of each array were moored in all tests. The connector stiffness is therefore expected to have less impact on module response of a two-module array, where both modules are moored, than for a five-module array with three middle modules held in place only by connectors. This can explain the similar surge motion at $K_c = S1$, $S2$ and $S3$ for two-module array, seen in Fig. 7(a). The softest spring, $S4$, yields a resonance peak at $T_w = 4.5$ s, coinciding with the calculated second natural period of the system, T_{n2}. Similar resonance peaks for the stiffer connection stiffnesses are visible, though less prominent.

Collisions between modules, as well as larger sway motion, were observed for some tests. The occurrence was most severe for the five-module configuration with the two softest springs $S3$ and $S4$. Ideally, the symmetrical model should show little to no sway motion when subjected to regular waves in the longitudinal direction. However, due to model asymmetries and low bending stiffness of the springs, collisions lead to transversal motion of some

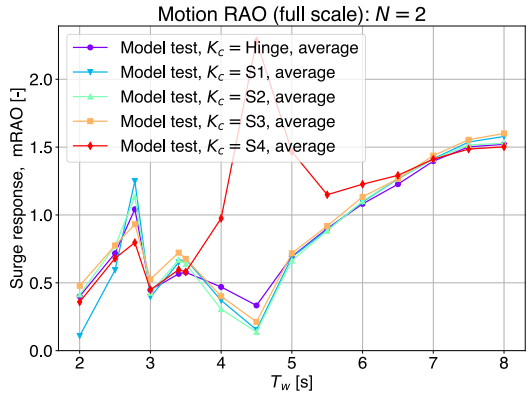

(a) N=2

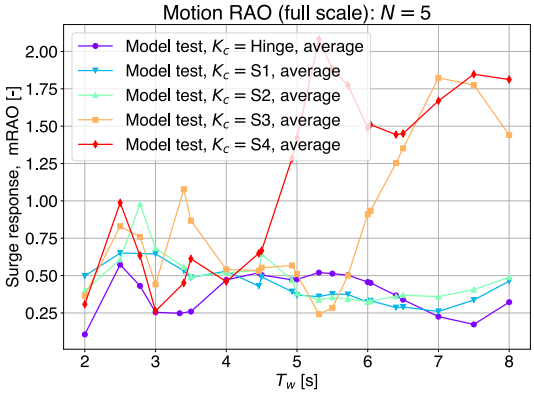

(b) N=5

Fig. 7. Average of response amplitude of all modules in surge.

modules. This nonlinear behavior became evident at $T_w = 6$ s for $S3$ and $T_w = 5.5$ s for $S4$, expected to be related to the second and third natural periods of the system. These larger amplitudes in surge are visible in Fig. 7(b). Hinged modules allow less relative motion, and the response is thus expected to be smaller, as seen in the same plot.

These results point to several potential control objectives: avoiding higher frequency loads, minimizing connector load, minimizing module motion or relative motion, closely related to moving the natural periods of the system away from the current sea state.

3.3 Comparison with Numerical Model

The hinged configuration is simulated by setting the connector stiffness high, $K_c = 4e5$. As seen in Fig. 8(a), the simulator is able to give a satisfactory estimation of the relative motion between hinged modules, a motion mainly occurring due to pitch motion. Further, as the connection springs get softer, there is a larger discrepancy between ex-perimental and numerical results. Fig. 9 shows the relative motion between modules for different connector stiffnesses. The peaks can be seen in relation with Tab. 4 as resonance peaks. The plots include a solid horizontal line indicating the collision limit.

The heave and pitch response for different connector stiffnesses are shown in Figs. 11(a) and 11(b) respectively. An

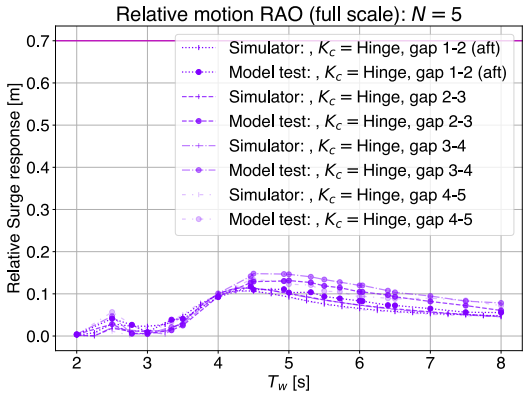

(a) Relative motion

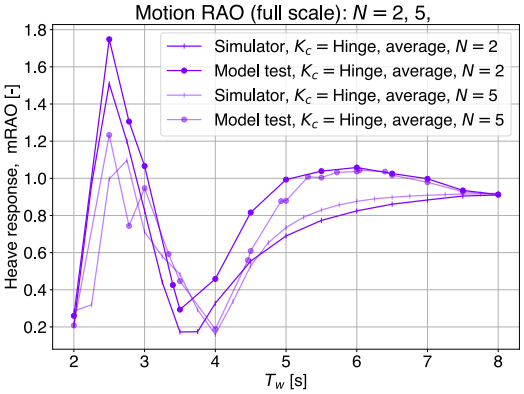

(b) Heave motion

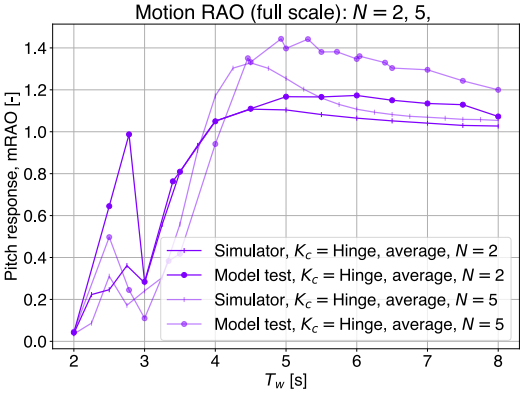

(c) Pitch motion

Fig. 8. Comparison of results with hinged modules.

average response is calculated from the motion amplitude of all modules. The heave response is mostly governed by potential forces, and not affected as much by the connections to other modules. The resonance peak corresponds to the calculated eigenperiod in heave for one module. The heave and pitch plots show a closer correspondence with the model test than the estimated surge motion and connector force shown in Fig. 10.

3.4 Error Sources

The main sources of discrepancy between the model test and the simulations are considered to be:

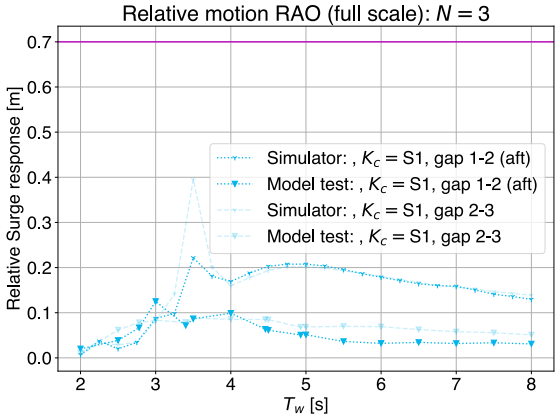

(a) $K_c = S1$

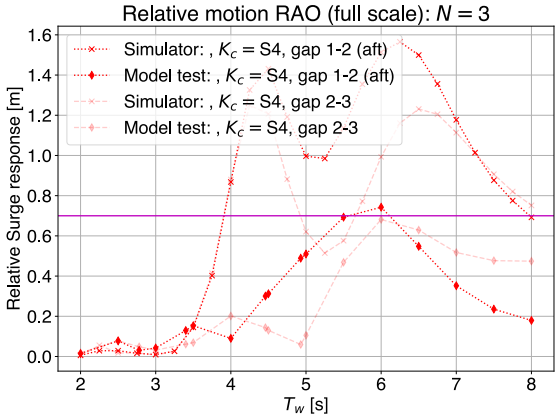

(b) $K_c = S4$

Fig. 9. Relative motion in surge between modules, N=3.

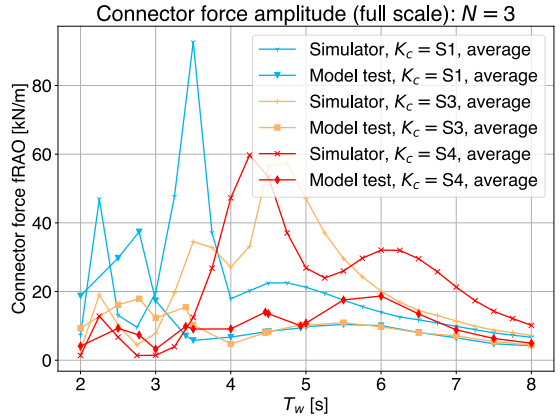

(a) Average connector force amplitude

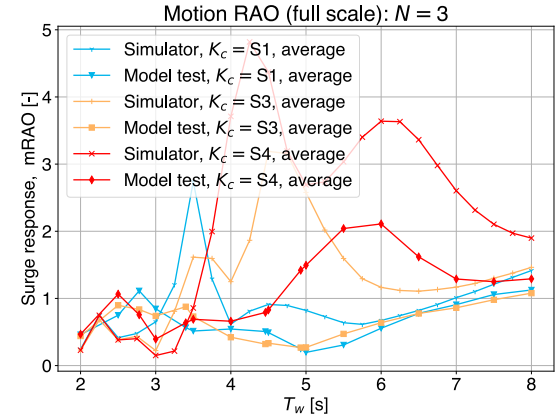

(b) Average response amplitude

Fig. 10. Comparison between experimental and numerical results, $N = 3$, at different connector stiffness K_c.

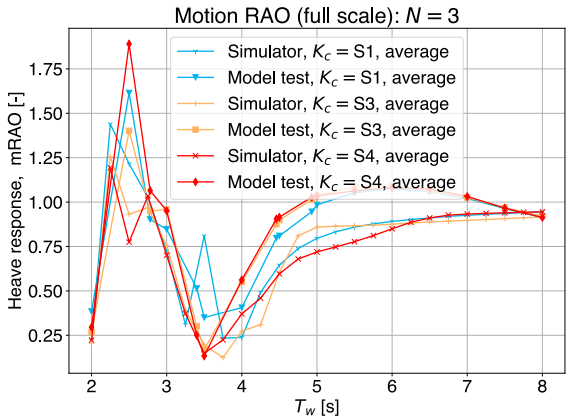

(a) Average heave amplitude, all modules.

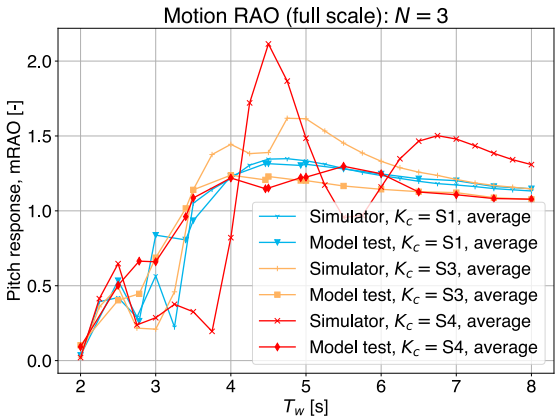

(b) Average pitch amplitude, all modules.

Fig. 11. Comparison between experimental and numerical results, N=3, heave and pitch response at different connector stiffness K_c.

- *Mooring line friction:* The mooring line in the model test included pulleys resulting in unmeasured friction and considerable added damping to the system. A corresponding force has not been included in the numerical model.
- *Nonlinear connector behavior:* The design of the connection springs only allowed for a known stiffness in the axial direction. The transversal and vertical, as well as the rotational stiffnesses are unknown. This leads to nonlinear behavior, especially for larger

waves and softer springs, that is not captured by the numerical model. The simulator does not seem to recreate the connector force measured in the model test well.

- *Collisions:* Collisions between modules and sway motion forced by the springs were observed for some runs.When collisions occur, forces in connections may be transferred to the module structure or to transversal motion without being measured, meaning that in these cases the load cells do not capture all interaction between neighboring modules.
- *Module overlap:* Related to collisions. Modules are allowed to overlap in the numerical simulations, meaning that response from the simulations can become large at resonance since the relative motion between modules is not limited by collisions.
- *Wake effects:* The design with several columns in close proximity of each other is expected to experience significant wake interaction, which is not considered in the simulator. These interactions will affect the hydrodynamic loads on the module columns, especially higher harmonic loads.

4. CONCLUSION

This paper has presented experimental and numerical analyses of a multi-modular floating structure, to investigate three main objectives: 1) Analyze the behavior of a multi-modular structure in changing wave conditions, 2) Investigate the effect of changing the stiffness of connectors between neighboring modules and 3) Validate a numerical simulator by comparable experimental results. First, choosing a spring connection with a proper stiffness instead of a hinged connection between modules appears to be beneficial to reduce connection loads between neighboring modules. When the array of modules is subjected to longer waves, a stiffer connection leads to a lower connection load, while at shorter waves a softer spring seems preferable. A softer spring shows fewer higher harmonic frequencies in the connection load than a hinge type connection. Choosing a softer spring in the connections could thus be beneficial if higher frequency loads are undesirable. The optimal stiffness for different sea states must be found as a balance between minimizing loads and staying within acceptable limits for module motion.

In general, the simulator proposed in this work overestimates load and response compared to model tests. The simulator does not capture the full dynamics shown by the model test and needs further investigation, especially considering the error sources mentioned in Sect. 3.4.

There is a significant amount of uncertainty related to the model tests, particularly related to connector design and mooring configuration. An improved connector design in future tests is necessary, and a mooring system without pulleys is preferable. Other possible topics for future experimental testing include investigating a 2D matrix of modules, changing wave angle, and including irregular sea states.

ACKNOWLEDGEMENTS

We would like to thank the engineers from NTNU IMT for all assistance during model tests.

REFERENCES

Ding, R., Yan, D.L., Zhang, H.C., Lu, Y., Shi, Q.J., Tian, C., Zhang, J.L., Ni, X.U., Xu, D.L., and Wu, Y.S. (2021). An application of network modeling method to scientific research and demonstration platform-connector load analysis. *Journal of Hydrodynamics 2021 33:1*, 33, 33–42. doi:10.1007/S42241-021-0011-2.

DNV (2022). The future of floating solar: Drivers and barriers to growth.

DNV-GL (2017). *SESAM USER MANUAL - WADAM - Wave Analysis by Diffraction and Morison theory*. DNV-GL, 9.3 edition.

Fagerbakke, V.N. (2023). *Enabling Intelligent Multi-Modular Concept for Solar Energy Harvest by Local Control of Connectors*. Master's thesis, NTNU.

Fossen, T. (2021). *Handbook of Marine Craft Hydrodynamics and Motion Control*. Wiley.

IPCC (2023). Sections. In: Climate Change 2023: Synthesis Report. Contribution of Working Groups I, II and III to the Sixth Assessment Report of the Intergovernmental Panel on Climate Change [Core Writing Team, H. Lee and J. Romero (eds.)]. 35–115. doi: 10.59327/IPCC/AR6-9789291691647.

Jiang, D., Tan, K.H., Wang, C.M., and Dai, J. (2021). Research and development in connector systems for very large floating structures. *Ocean Engineering*, 232, 109150. doi:10.1016/J.OCEANENG.2021.109150.

Kumar, M., Niyaz, H.M., and Gupta, R. (2021). Challenges and opportunities towards the development of floating photovoltaic systems. *Solar Energy Materials and Solar Cells*, 233, 111408. doi: 10.1016/J.SOLMAT.2021.111408.

Lamas-Pardo, M., Iglesias, G., and Carral, L. (2015). A review of very large floating structures (vlfs) for coastal and offshore uses. *Ocean Engineering*, 109, 677–690. doi: 10.1016/J.OCEANENG.2015.09.012.

Onsrud, M. (2019). *An Experimental Study on the Wave-Induced Vertical Response of an Articulated Multi-Module Floating Solar Island*. Master's thesis, NTNU.

Shi, Q.J., Zhang, H.C., Xu, D.L., Qi, E.R., Tian, C., Ding, J., Wu, Y.S., Lu, Y., and Li, Z.W. (2018). Experimental validation of network modeling method on a three-modular floating platform model. *Coastal Engineering*, 137, 92–102. doi:10.1016/j.coastaleng.2018.04.001.

Xia, S.Y., Xu, D.L., Zhang, H.C., Qi, E.R., Hu, J.J., and Wu, Y.S. (2016). On retaining a multi-module floating structure in an amplitude death state. *Ocean Engineering*, 121, 134–142. doi:10.1016/j.oceaneng.2016.05.024.

Xu, D.L., Zhang, H.C., Qi, E.R., Hu, J.J., and Wu, Y.S. (2014). On study of nonlinear network dynamics of flexibly connected multi-module very large floating structures. doi:10.1061/9780784413609.181.

Zhang, H.C., Xu, D.L., Lu, C., Qi, E.R., Tian, C., and Wu, Y.S. (2017). Connection effect on amplitude death stability of multi-module floating airport. *Ocean Engineering*, 129, 46–56. doi:10.1016/j.oceaneng.2016.11.011.

Zhang, H.C., Xu, D.L., Xia, S.Y., Lu, C., Qi, E.R., Tian, C., and Wu, Y.S. (2015). Nonlinear network modeling of multi-module floating structures with arbitrary flexible connections. *Journal of Fluids and Structures*, 59, 270–284. doi:10.1016/j.jfluidstructs.2015.09.012.